Molecules and Cells

Molecular Signatures of Sinus Node Dysfunction Induce Structural Remodeling in the Right Atrial Tissue

Seung-Young Roh[1,5], Ji Yeon Kim[2,5], Hyo Kyeong Cha[2], Hye Young Lim[2], Youngran Park[2], Kwang-No Lee[3], Jaemin Shim[3], Jong-Il Choi[3], Young-Hoon Kim[3,*], and Gi Hoon Son[2,4,*]

[1]Division of Cardiology, Department of Internal Medicine, Korea University College of Medicine and Korea University Guro Hospital, Seoul 08308, Korea, [2]Department of Biomedical Sciences, College of Medicine, Korea University, Seoul 02841, Korea, [3]Division of Cardiology, Department of Internal Medicine, Korea University College of Medicine and Korea University Anam Hospital, Seoul 02841, Korea, [4]Department of Legal Medicine, College of Medicine, Korea University, Seoul 02841, Korea, [5]These authors contributed equally to this work.
*Correspondence: songh@korea.ac.kr (GHS); yhkmd@unitel.co.kr (YHK)
https://doi.org/10.14348/molcells.2020.2164
www.molcells.org

The sinus node (SN) is located at the apex of the cardiac conduction system, and SN dysfunction (SND)—characterized by electrical remodeling—is generally attributed to idiopathic fibrosis or ischemic injuries in the SN. SND is associated with increased risk of cardiovascular disorders, including syncope, heart failure, and atrial arrhythmias, particularly atrial fibrillation. One of the histological SND hallmarks is degenerative atrial remodeling that is associated with conduction abnormalities and increased right atrial refractoriness. Although SND is frequently accompanied by increased fibrosis in the right atrium (RA), its molecular basis still remains elusive. Therefore, we investigated whether SND can induce significant molecular changes that account for the structural remodeling of RA. Towards this, we employed a rabbit model of experimental SND, and then compared the genome-wide RNA expression profiles in RA between SND-induced rabbits and sham-operated controls to identify the differentially expressed transcripts. The accompanying gene enrichment analysis revealed extensive pro-fibrotic changes within 7 days after the SN ablation, including activation of transforming growth factor-β (TGF-β) signaling and alterations in the levels of extracellular matrix components and their regulators. Importantly, our findings suggest that periostin, a matricellular factor that regulates the development of cardiac tissue, might play a key role in mediating TGF-β-signaling-induced aberrant atrial remodeling. In conclusion, the present study provides valuable information regarding the molecular signatures underlying SND-induced atrial remodeling, and indicates that periostin can be potentially used in the diagnosis of fibroproliferative cardiac dysfunctions.

Keywords: cardiac fibrosis, periostin, right atrium, sinus node dysfunction, transcriptome, transforming growth factor-β

INTRODUCTION

The sinus node (SN) located in the superior right atrium (RA) is the uppermost part of the cardiac conduction system. SN dysfunction (SND) characterized by electrical remodeling has usually been attributed to age-related idiopathic fibrosis or ischemic injuries in the SN (John and Kumar, 2016). The prevalence of SND is estimated to be 1 per 1,000 person-years in individuals over 45 years of age. Its incidence

Received 22 July, 2019; revised 30 January, 2020; accepted 5 March, 2020; published online 31 March, 2020

eISSN: 0219-1032

increases during aging, occurring in 1 among 600 patients over 65 years of age (Dobrzynski et al., 2007; Jensen et al., 2014). SND is associated with increased risk of cardiovascular disorders, including syncope, heart failure, and atrial arrhythmias (Alonso et al., 2014). It is the most common indication for the implantation of an artificial pacemaker, and accounts for 30% to 50% of all implants in the USA (Abe et al., 2014; Bernstein and Parsonnet, 1996). SND and atrial arrhythmias, in particular atrial fibrillation (AF), frequently coexist in the elderly (Andersen et al., 1997; Connolly et al., 2000). In large population studies, the risk of AF onset among patients with SND has been estimated to be > 4-fold higher than that in normal individuals (Lamas et al., 2002; Nielsen et al., 2011). Recent studies have advanced our understanding of the pathophysiological and molecular mechanisms underlying the development and progression of SND and AF (Joung et al., 2010; Li et al., 2011; Ziyadeh-Isleem et al., 2014).

One of the histological hallmarks of SND is degenerative atrial remodeling, characterized by structural changes, conduction abnormalities, and increased right atrial refractoriness (Sanders et al., 2004). Bradycardia caused by electrical remodeling or pressure overload after heart failure may impact the atrial remodeling. Notably, SND is accompanied by structural changes in the RA such as increased atrial fibrosis along with accumulation of collagen deposits (John and Kumar, 2016; Sanders et al., 2004). Collagen accumulation replaces the degenerating myocardium, which often leads to cardiac hypertrophy (Assayag et al., 1997; Silver et al., 1990). In human hearts, senescence-related atrial fibrosis correlates well with impaired heart rate (HR) and prolonged sinoatrial conduction time (John and Kumar, 2016; Sanders et al., 2004). Despite the strong correlation between SND and atrial remodeling, the molecular and cellular bases underlying SND-induced structural remodeling remain to be elucidated.

The present study examined whether SND could induce significant changes in the RA at the molecular level that may account for the structural remodeling. For this purpose, we developed a rabbit model of experimental SND and then compared the transcriptome profiles of the RA between SND-induced and sham-operated animals to identify the differentially expressed gene (DEG) transcripts and to evaluate their functional relevance.

MATERIALS AND METHODS

Animals and SND modeling

New Zealand white rabbits (3-3.5 kg) used in this study were obtained from Central Laboratory Animals Inc. (Korea). Male rabbits were housed at 22°C to 23°C and 50% humidity under a 12 h light/dark photoperiod (lights on at 08:00 a.m.) with free access to food and water. The rabbit SND model was established as per previously published protocols with minor modifications (Liu et al., 2012). Briefly, rabbits were anesthetized with 35 mg/kg ketamine, 5 mg/kg xylazine, and 1% to 4% isoflurane. Tracheal intubation and respiration assistance were provided with blood pressure and PaO_2 monitoring. The heart was exposed by right-thoracotomy. To induce the experimental SN damage (SNX), a 3 mm diameter cotton ball soaked in 20% formaldehyde (Sigma-Aldrich, USA) was placed on the SN region between the RA and superior vena cava until a junctional rhythm or significant sinus bradycardia with an HR of 100 beats/min (bpm) was generated. Saline was used instead of formaldehyde for sham-operated controls. Then, the implantable loop recorder (Reveal® XT; Medtronic, USA) was inserted and fixed in the subcutaneous layer of the right chest to measure HR. The ventricular tachycardia zone of the loop recorder was set at HR > 130 bpm and the duration spent at HR > 130 bpm was recorded for successive 7 days. After the 7-day HR measurement, the animals were euthanized and myocardial tissues were isolated as follows: RA-free wall near the RA appendage, left atrial (LA) posterior wall, right ventricle (RV) mid-free wall, and left ventricular (LV) mid-free wall. All the animal experiments were approved by the Institutional Animal Care and Use Committee of Korea University, Seoul, Korea (KUIACUC-2015-46).

Histological examination

Isolated cardiac tissues were subjected to alcoholic dehydration and embedded in paraffin after fixation with 4% paraformaldehyde in phosphate-buffered saline for 24 h. Serial sections were prepared at 6 μm, and stained with H&E according to the standard protocol. Heart tissue sections were also subjected to Masson's trichrome staining (MTS) to assess fibrotic lesions in accordance to a previously described protocol (Zhao et al., 2018).

Transcriptome analysis

Total RNA was extracted from 30 to 50 mg RA tissue using RNeasy Mini kits according to the manufacturer's instructions (Qiagen, Germany) and RNA integrity was evaluated with an Agilent 2100 Bioanalyzer (Agilent, USA). Total RNA sequencing (RNA-Seq) for transcriptome profiling and subsequent gene enrichment analysis were carried out as previously described with minor modifications (Chung et al., 2016; Kim et al., 2018). Briefly, total RNA was subjected to ribosomal RNA depletion with Ribo-Zero reagent and then cDNA libraries were prepared using the TruSeq Stranded Total RNA prep kit according to the manufacturer's instructions (Illumina, USA). Primary sequence data were acquired using paired-end sequencing by HiSeq 2500 sequencing platform (Illumina), and raw reads were then pre-processed by removing the adapter and low-quality sequences (< Q20) by using Trimmomatic with default parameters. TopHat (ver. 2.0.13; http://ccb.jhu.edu/software/tophat/) and Cuffdiff (ver. 2.2.0; http://cole-trapnell-lab.github.io/cufflinks/cuffdiff/) were used to map the processed reads to the rabbit reference genome (Ensembl OryCun2.0.84) and to obtain transcript abundance in FPKM > 2 and analyze the DEGs, respectively. DEGs with > 2-fold changes at $P < 0.05$ by Student's *t*-test were used to construct a primary dataset. Selected DEGs were then filtered by enrichment in "heart" or "cardiomyocyte" in the Ingenuity knowledge database and analyzed by the "core analysis" function of Ingenuity Pathway Analysis (IPA) (Qiagen; http://www.ingenuity.com). We mainly utilized "Canonical pathway analysis", "Biological functions and diseases annotation," and "Upstream regulators" functions of the IPA to explore pathway enrichment and to predict alterations in atrial functions.

Quantitative reverse transcription-polymerase chain reaction

For the selected DEGs identified by the transcriptome analysis, we validated alterations in expression using quantitative reverse transcription-polymerase chain reaction (qRT-PCR) as described previously (Chung et al., 2016). We reverse-transcribed 500 ng RNA with MMLV reverse transcriptase (Promega, USA). The resulting cDNA was subjected to qPCR with SYBR Green I and ROX (as a passive dye) (Sigma-Aldrich). Glyceraldehyde-3-phosphate dehydrogenase (*GAPDH*), peptidylprolyl isomerase A (*PPIA*), and TATA-binding protein (*TBP*) genes were employed as the internal controls, and the average expression levels of the three genes were used to normalize the relative expression of the target genes. The primers used for qRT-PCR are as follows: *rGAPDH* forward, 5′-TCT GGC AAA GTG GAT GTT GT-3′; *rGAPDH* reverse, 5′-TGG GTG GAA TCA TAC TGG AA-3′; *rPPIA* forward, 5′- AAG CAC ACA GGT CCT GGC AT-3′; *rPPIA* reverse, 5′-CTC GGA CCC AAA GTG CTC CA-3′; *rTBP* forward, 5′-CTT ACA ACC GCA CCC TTG CC-3′; *rTBP* reverse, 5′-TTC GGG CAC GAA GTG CAA TG-3′; *rTGF-β1* forward, 5′-CCT CTG GAA CGG GCT CAA CA-3′; *rTGF-β1* reverse, 5′- GAC TCT CCG CTC CGG TAC AC-3′; *rCTGF* forward, 5′-ACC CGC ACA AGG GAC TCT TC-3′; *rCTGF* reverse, 5′-GAC TCT CCG CTC CGG TAC AC-3′; *rIGF1* forward, 5′-GCA TCC TGT CCT CCT CGC AT-3′; *rIGF1* reverse, 5′-TGC TGG AGC CGT ATC CTG TG-3′; *rPOSTN* forward, 5′-GGT CTT GGC TCA TAG CCG TAT CA-3′; *rPOSTN* reverse, 5′-TCC CGC ATA TGG CAC CTT GG-3′; *rNPR1* forward, 5′-TGC AGA GCC ACA TGG AGG AG-3′; *rNPR1* reverse, 5′-TCA GGC GGA TCT GCT GGA AG-3′; *rTNFRSF1A* forward, 5′-TTG GTC TGT GCC TGC TCT CC-3′; *rTNFRSF1A* reverse, 5′-ACA GGT GTC GCT TTC CCA CA-3′; *rTRAF3* forward, 5′-GCC GAC AGC ATG AAG AGC AG-3′; *rTRAF3* reverse, 5′-TCA GCT GGG ACT CCA GCA AG-3′; *rITGB2* forward, 5′-GCC CTC AAC GAG ATC ACC GA-3′; *rITGB2* reverse, 5′-AGC ACC GTC TTG TCC ACG AA-3′; *rVCAM1* forward, 5′-GCG GAG ACA GGA GAC ACA GT-3′; *rVCAM1* reverse, 5′-AGA GCA CGA GAA GTT CAG GAG AAA-3′; *rFN1* forward, 5′-CAG CAG TAC GGC CAC AGA GA-3′; *rFN1* reverse, 5′-GTG TCG GAA GCT GAG ACC CA-3′; *rFBN1* forward, 5′-CTG GCC TCA GAT GGG CGT TA-3′; *rFBN1* reverse, 5′-TGT CGA CAC ACA CAC GTC CA-3′; *rCOL3A1* forward, 5′-TAT TCC TGG CCA GCG AGG TG-3′; *rCOL3A1* reverse, 5′-AGG TGA GCC GTC TTT GCC AT-3′; *rCOL5A1* forward, 5′-ATC GCT CTC AGC GTC CAC AA-3′; *rCOL5A1* reverse, 5′-CGG GTC CCG AAC ACG ATG AT-3′; *rWISP1* forward, 5′-TGG AGC CAA GCA CCA CGT TA-3′; *rWISP1* reverse, 5′-TCC CAG CTT CCT GGA GTC CT-3′; *rMMP2* forward, 5′-TGG TGC TGC CAC ACT TGA GA-3′; *rMMP2* reverse, 5′-AAG GCA GCC AGC AGT GAG AA-3′; *rLOX* forward, 5′-GAG GAG GGT GGC TGA AGG TC-3′; *rLOX* reverse, 5′-AAT GTA GTT GCC GGG CTG GA-3′; *rACTA1* forward, 5′-AGG GCG TCA TGG TGG GTA TG-3′; *rACTA1* reverse, 5′-GCC GTG CTC GAT GGG ATA CT-3′; *rACTA2* forward, 5′-CAC TGC TGC ATC CTC CTC CT-3′; *rACTA2* reverse, 5′-GAG GGC TGG AAC AGG GTC TC-3′; *rACTG2* forward, 5′-TGC GGG TAG CAC CTG AAG AG-3′; *rACTG2* reverse, 5′-TTC TCC CTG TTG GCC TTG GG-3′; *rSIRT1* forward, 5′-GGC CGG AGG AGA CAA TGG G-3′; *rSIRT1* reverse, 5′-TCG TCG TCT TCG TCT TCG CA-3′; *rRCAN1* forward, 5′-TTG TCC CAG TCC GTG TGC TT-3′; *rRCAN1* revers, 5′-CGC TAC TGT GAC CGG TTT GC-3′.

Immunoblotting

Anti-periostin (sc49480; Santa Cruz, USA), anti-TGF-β1 (MA5-16949; Invitrogen, USA), and β-actin (A2228; Sigma-Aldrich) antibodies were commercially obtained. Immunoblotting and accompanying densitometric analyses were carried out as described previously (Chung et al., 2017). Whole-cell extracts were resolved on sodium dodecyl sulfate-polyacrylamide gels and transferred onto polyvinylidene fluoride membranes (Millipore, USA). The blots were blocked with Tris-buffered saline containing 0.3% Tween 20 and 3% bovine serum albumin and incubated with the primary antibodies at room temperature for 1 h. Antibody binding was detected by incubation with secondary antibodies linked to horseradish peroxidase (Jackson ImmunoResearch Laboratories, USA) accompanied by visualization using enhanced chemiluminescence reagents (Thermo Fisher Scientific, USA). Optical densities of immunoreactive bands were quantified using NIH ImageJ software (http://rsb.info.nih.gov/ij/), and the relative amounts of the target proteins were deduced by comparing with the optical band densities of the serially diluted reference extracts.

Data analysis

Results are expressed as mean ± SEM. Differences in HR measurement, qRT-PCR, and immunoblotting analyses between groups were statistically evaluated using unpaired Student's *t*-test. A P value < 0.05 was considered significant.

RESULTS

Experimental SND induced cardiac dysfunctions

Among the original 13 rabbits subjected to SNX, seven animals survived and five were successfully modeled for SND. The mean baseline HRs of the rabbits with SNX did not significantly differ from those observed in control (CTL) animals before modeling (183.67 ± 3.48 bpm for CTL vs 184.20 ± 4.26 bpm for SNX, P = 0.934; Fig. 1A, upper panel). The model achievement rate calculated by % duration spent at HR < 130 bpm was 88.57% ± 4.68% in the SNX animals, compared with 1.79% ± 0.34% for controls (P < 0.01; Fig. 1A, lower panel). AF was not significantly observed in any of the animals during the 7-day analysis. After SND modeling, RA tissue sections were stained with H&E (Fig. 1B, upper panel) and MTS (Fig. 1B, lower panel). The atria of rabbits with SNX were histologically characterized by expanded fibrotic area stained blue by MTS (Fig. 1B, lower panel). These results indicate that impaired SN function leads to the structural remodeling of RA in association with atrial fibrosis and bradycardia regardless of AF.

SN ablation induces alterations in the RNA expression profiles of RA tissues

To explore the molecular signatures underlying SNX-induced atrial remodeling, we compared the genome-wide RNA expression profiles of RA tissues from CTL and SNX rabbits by RNA-Seq. We identified 641 DEG transcripts between

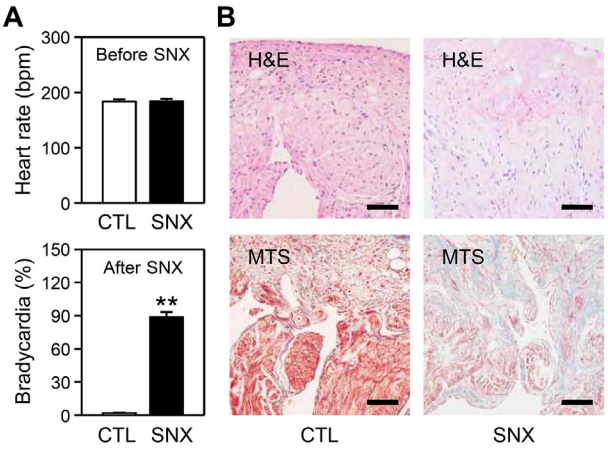

Fig. 1. Cardiac dysfunctions induced by sinus node damage. (A) Average heart rate (HR) before the experimental sinus node damage (SNX; upper panel), and the duration (%) for which bradycardia is exhibited 7 days after SND induction (lower panel) in comparison with that in sham-operated controls (CTL). Sinus bradycardia was considered developed at HR < 130 bpm. Data are expressed as mean ± SEM (n = 3 for CTL and 5 for SNX groups; $**P < 0.01$ by *t*-test). (B) Increased fibrosis in the RA tissues by SNX. The RA sections were stained with H&E (upper panel) or MTS (lower panel). Scale bars = 50 μm.

the two groups. The top 30 mRNA species differentially expressed at the highest levels are shown (Fig. 2 and Supplementary Table S1 for the full list of the DEGs). It is noteworthy that the expression of gene transcripts coding for the extracellular matrix (ECM) components and their regulators such as macrophage collagens (COLs), fibronectin 1 (FN1), and metalloelastases (MMPs) suggests the structural remodeling of myocardium. To gain more systemic insights, we next categorized the DEGs set using IPA. The IPA canonical pathway analysis on the DEGs revealed significantly enriched pathways in the SNX RA, including the GP6 (Glycoprotein 6) signaling pathway, actin cytoskeleton signaling, TREM1 (Triggering receptor expressed on myeloid cells 1) signaling, Rac signaling, and neuroinflammation signaling (Table 1). Furthermore, these canonical pathways were significantly biased towards activation (Z-scores > 2.0 for the top 10 pathways listed in Table 1). To further examine the functional impact of SNX, we also used the functional analysis tools of IPA to analyze the DEGs. In the enrichment analysis by biological functions/diseases in the IPA, inflammatory response in the category of "Diseases and disorders", cellular movement in "Molecular and cellular functions", and cardiovascular system and function in "Physiological system development and function" were the most significant terms in each category (Table 2). IPA analysis for upstream regulators predicted by DEGs suggested TGF-β1 (transforming growth factor beta 1 coded

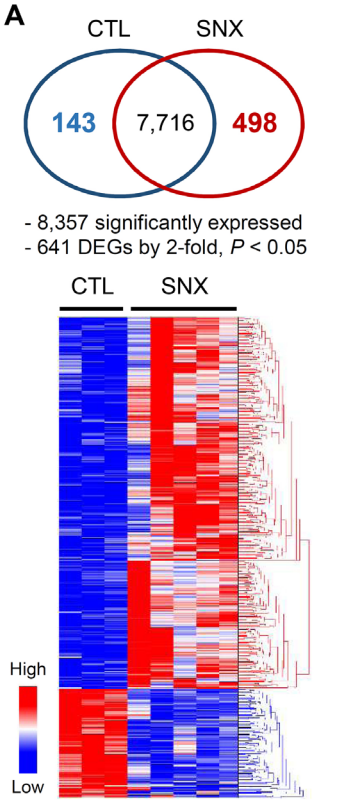

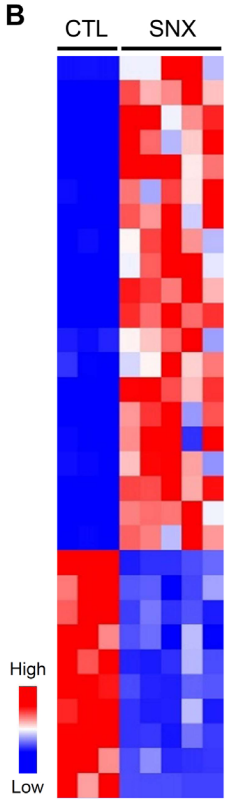

Symbol	Fold	Gene description
MMP12	917.65	Macrophage metalloelastase 12
CEP55	224.71	Centrosomal protein 55kDa
POSTN	141.74	Periostin, osteoblast specific factor
COL11A1	33.86	Collagen, type XI, alpha 1
COL12A1	32.30	Collagen, type XII, alpha 1
TNC	31.58	Tenascin C
ACAN	28.36	Aggrecan
RRM2	26.52	Ribonucleotide reductase M2
GPNMB	24.34	Glycoprotein (transmembrane) nmb
CENPF	22.90	Centromere protein F
FN1	22.28	Fibronectin 1
CDK1	21.98	Cyclin-dependent kinase 1
P4HA3	20.58	Prolyl 4-hydroxylase, alpha polypeptide III
ADAM12	20.29	ADAM metallopeptidase domain 12
WISP1	20.17	WNT1 inducible signaling pathway protein 1
LTBP2	19.74	Latent TGF beta binding protein 4
ARNTL2	19.11	ARNT like 2
MKI67	18.08	Marker of proliferation Ki-67
HAS2	17.56	Hyaluronan synthase 2
NCAPG	16.78	Non-SMC condensin I complex subunit G
LIPE	-4.54	Lipase, hormone-sensitive
COL4A6	-4.90	Collagen, type IV, alpha 6
CDO1	-6.32	Cysteine dioxygenase type 1
CNTN1	-6.38	Contactin 1
OPCML	-8.42	Opioid binding protein/cell adhesion molecule-like
DLG2	-8.52	Discs, large homolog 2 (Drosophila)
CPNE5	-10.26	Copine V
CEP126	-13.13	Centrosomal protein 126kDa
CIDEA	-13.52	Cell death-inducing DFFA-like effector a
THRSP	-86.93	Thyroid hormone responsive

Fig. 2. Genome-wide RNA expression profiles in RA tissues. (A) Venn diagram (upper panel) and heat map representation with hierarchical clustering (lower panel) of the differentially expressed genes (DEGs) examined 7 days after SNX. RNA levels of 143 genes were significantly higher in the sham-operated controls (CTLs), and 498 RNA levels were higher in the rabbits with SNX. (B) Heat map representation of the top 30 DEGs.

Table 1. Top canonical pathways

Ingenuity canonical pathway	*P* value[a]	*Z* score[b]	Overlap
GP6 signaling pathway	5.89E-06	4.00	16/82 (0.195)
Actin cytoskeleton signaling	1.00E-05	3.44	23/157 (0.146)
Th17 activation pathway	2.24E-05	2.33	10/38 (0.263)
Leukocyte extravasation signaling	6.76E-05	3.90	19/131 (0.145)
ILK signaling	8.32E-05	2.67	20/144 (0.139)
Macropinocytosis signaling	1.29E-04	2.65	12/64 (0.188)
TREM1 signaling	2.63E-04	3.00	9/41 (0.220)
Rac signaling	2.95E-04	3.61	14/90 (0.156)
Agrin interactions at neuromuscular junction	4.47E-04	3.16	10/53 (0.189)
Neuroinflammation signaling	5.75E-04	3.27	22/191 (0.115)

[a]$P < 0.05$ by Fisher's exact test. [b]|Activation *Z* score| > 2.

Table 2. Top diseases and biological functions

Category	*P* value[a]	No. of molecules
Diseases and disorders		
Inflammatory response	1.70E-06 - 1.50E-18	208
Developmental disorder	2.53E-06 - 3.48E-17	72
Hereditary disorder	2.53E-06 - 3.48E-17	116
Organismal injury and abnormalities	2.55E-06 - 3.48E-17	442
Skeletal and muscular disorder	2.53E-06 - 3.48E-17	184
Molecular and cellular functions		
Cellular movement	1.99E-06 - 5.12E-28	209
Cell-to-cell signaling and interaction	2.46E-06 - 8.25E-16	151
Cellular development	2.35E-06 - 1.42E-14	212
Cellular assembly and organization	1.31E-06 - 2.96E-12	80
Cellular function and maintenance	2.04E-06 - 2.96E 12	152
Physiological system development and function		
Cardiovascular system and function	1.48E-06 - 2.58E-20	157
Organismal development	1.51E-06 - 2.58E-20	207
Tissue development	1.84E-06 - 1.36E-19	233
Connective tissue development and function	1.84E-06 - 3.13E-19	161
Skeletal & muscular system development and function	2.27E-06 - 3.13E-19	108

[a]$P < 0.05$ by Fisher's exact test.

Table 3. Top 10 upstream regulators with altered mRNA expression

Symbol	FC[a]	Type	*P* value[b]	*Z* score[c]	No. of targets
TGFB1	3.05	Growth factor	2.19E-29	5.52	80
AHR	2.99	Nuclear receptor	1.77E-11	2.56	36
CTGF	4.48	Growth factor	2.77E-09	2.08	15
IL6R	2.39	Transmembrane receptor	1.29E-08	2.02	11
SPP1	9.27	Cytokine	1.11E-07	2.31	17
HIF1A	2.79	Transcription regulator	1.15E-07	3.27	32
FBN1	2.82	Other	1.50E-07	2.61	8
ETV5	2.60	Transcription regulator	3.13E-06	2.33	13
FN1	22.28	Enzyme	1.09E-05	2.20	8
FOXM1	3.55	Transcription regulator	1.19E-05	3.48	14

[a]Fold changes (FCs) in mRNA expression. [b]$P < 0.05$ by Fisher's exact test. [c]|Activation *Z* score| > 2.

by *TGFB1*) as one of the top activated upstream regulators in the SNX RA tissues (Table 3). It is interesting that several downstream targets of TGF-β signaling, such as *CTGF* (connective tissue growth factor), *FN1*, *FBN1* (fibrillin 1), *SPP1* (secreted phosphoprotein 1), *COL18A1*, and *POSTN* (coding for periostin) were included in the upstream regulators sig-

nificantly activated or inhibited in the SNX RA (Table 3 and Supplementary Table S2 for the extended list of the target genes). This observation also supports the fact that the TGF-β signaling cascade was activated. Collectively, these findings suggest that remodeling of intracellular cytoskeleton as well as the ECM, along with inflammatory responses may occur in the RA tissue upon SN ablation, and the TGF-β signaling cascade may play a role in mediating these processes.

We then focused on the 21 DEGs belonging to at least one functional category listed in Tables 2 and 3 and validated their expression patterns by qRT-PCR (Fig. 3). Fifteen of these genes were categorized as downstream targets of TGF-β signaling in the IPA. Among the significantly upregulated transcripts, *CTGF*, *IGF1*, and *POSTN* code for secretory factors, implying their mediatory roles in amplifying the actions of TGF-β. Concordantly, TGF-β–responsive mRNA species that are responsible for ECM organization, such as *FN1*, *FBN1*, *COL3A1*, *COL5A1*, *MMP2*, *ITGB2* (integrin β2), and *LOX* (lysyl oxidase) as well as several actin subunits, including *ACTA1*, *ACTA2*, and *ACTG2* were significantly upregulated by experimental SND. The expression of additional ECM organizing factors such as *WISP1* (WNT1-inducible-signaling pathway protein 1) and *VCAM1* (vascular cell adhesion molecule 1), and inflammation-mediating factors such as *TNFRSF1A* (TNF receptor superfamily member 1A), *TRAF3* (TNF receptor-associated factor 3), and *RCAN1* (regulator of calcineurin 1) was also significantly higher in the SNX than that in the CTL animals. By contrast, mRNA expression of protective factors that suppress cardiac fibrosis and hypertrophy such as *NPR1* (natriuretic peptide receptor 1) and *SIRT1* (sirtuin 1) was significantly reduced in the SNX group.

Expression of periostin protein in the myocardial tissues

It should be noted that *POSTN* mRNA levels were drastically increased in the RA of SNX animals (141.74 ± 17.05 and 126.86 ± 22.12 folds by RNA-Seq and qRT-PCR, respectively). Therefore, we compared the expression profiles of periostin and TGF-β1 proteins in various cardiac tissues between the SNX and control rabbits. Immunoblot analyses revealed a dramatic increase (> 10-fold in signal intensity) in periostin protein levels in the SNX RA lysates, while TGF-β1 showed a modest increase of approximately 2-fold (Fig. 4). More importantly, the levels of periostin protein were significantly higher in all the tested cardiac tissues from the SNX group than in those from the CTL group. In contrast to those of periostin, the protein levels of TGF-β1 showed a tendency to increase in the LA, but they were not significantly different between the groups. Furthermore, the levels of TGF-β1 protein drastically decreased in the RV tissues and showed a tendency to decrease in the LV in response to SNX (Fig. 4B).

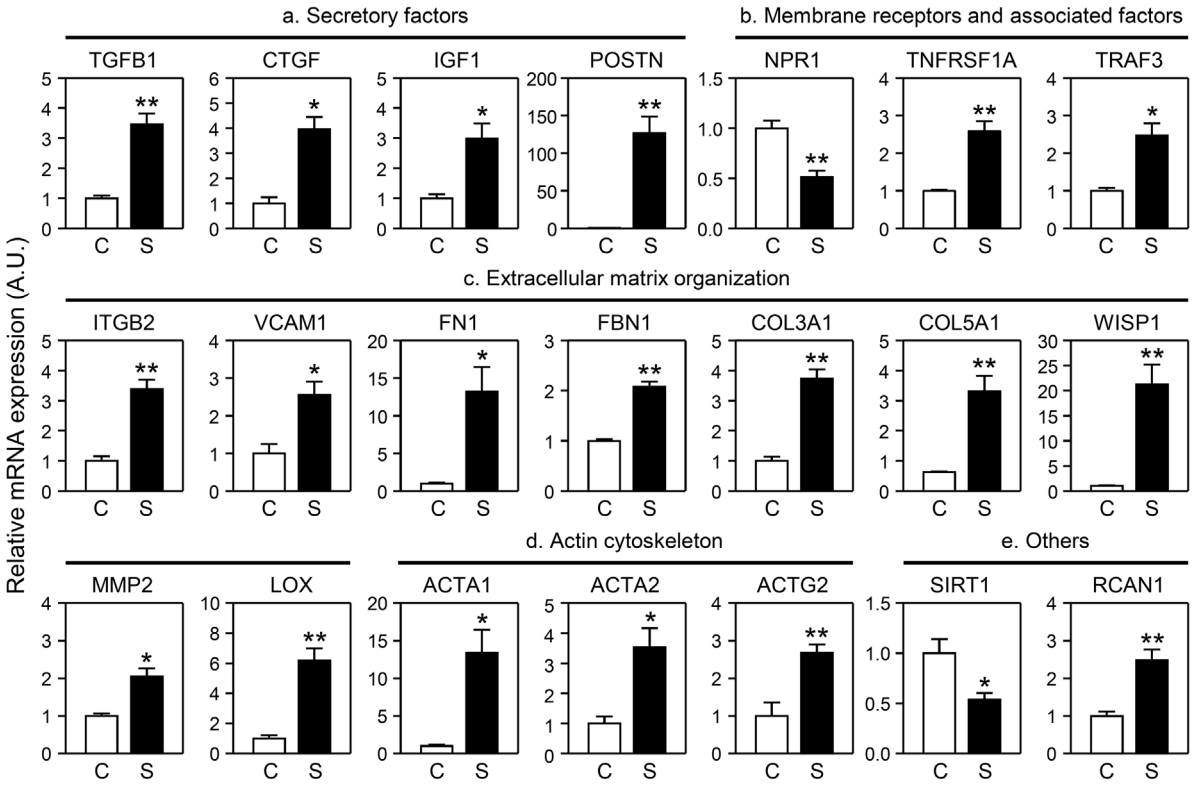

Fig. 3. Validation of the differential expression of selected mRNA species. qRT-PCR analyses of the selected DEGs categorized as secretory factors (a), membrane receptors and associated proteins (b), factors involved in extracellular matrix organization (c), actin cytoskeletal subunits (d), and other regulatory factors (e). Relative expression of each mRNA species was normalized to that of the average GAPDH, PPIA, and TBP expression and presented as mean ± SEM in arbitrary units (A.U.), for which the mean expression in the control (CTL) was defined as 1 (n = 3 for CTL [C] and 5 for SND [S] groups; $*P < 0.05$ and $**P < 0.01$ by unpaired *t*-test).

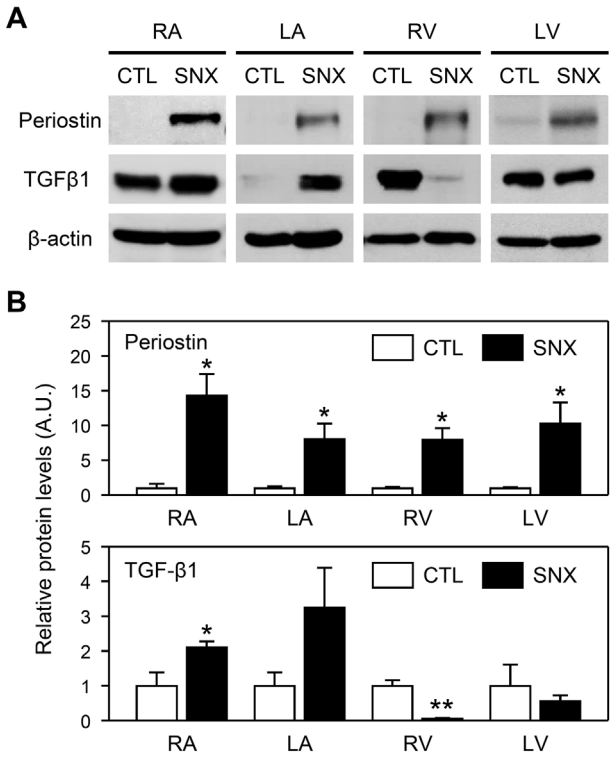

Fig. 4. Periostin and TGF-β1 expression at protein levels in cardiac tissues. (A) Representative images depicting the expression of periostin, TGF-β1, and β-actin proteins in various myocardial tissues as evaluated by immunoblot (RA, right atrium; LA, left atrium; RV, right ventricle; LV, left ventricle). (B) Expression of periostin and TGF-β1 proteins normalized to that of β-actin is presented as mean ± SEM in arbitrary units (A.U.), for which the mean expression in the control (CTL) was defined as 1 (n= 3 for CTL and 5 for the SNX groups; $*P < 0.05$ and $**P < 0.01$ by unpaired *t*-test).

Although the expression of periostin in cardiac fibrosis has been linked with TGF-β signaling, our results clearly show more robust and consistent changes in periostin protein expression in all myocardial tissues in response to SND.

DISCUSSION

In the present study, we successfully induced the cardiac dysfunctions characterized by bradycardia as well as atrial fibrosis in a rabbit model of SND and then identified a set of genes whose transcripts exhibited altered expression in the RA. In agreement with increasing evidence—from both experimental and clinical studies—that indicates a close relationship between SND, AF, and atrial fibrosis (John and Kumar, 2016), we clearly showed that impaired SN function leads to a huge change in the expression of genes, particularly those related to the structural remodeling of RA within 7 days after SNX. Considering that a clear AF was not observed in our model, the fibrotic remodeling in RA appears to be induced by the experimental SND regardless of the onset of AF.

Our transcriptome analysis revealed that > 75% of the DEGs showed increased expression in the SNX group, and subsequent gene enrichment analysis suggested that extensive ECM remodeling occurred in the RA tissue. Indeed, more than half of the top 20 upregulated DEGs listed in Fig. 2B—*MMP12*, *CEP55*, *POSTN*, *COL11A1*, *COL12A*, *TNC*, *ACAN*, *FN1*, *ADAM12*, *WISP1*, and *LTBP2*—are involved in regulation of ECM remodeling. It is noteworthy that the target genes of TGF-β signaling—shown in Fig. 3—also include important regulators of ECM organization including *ITGB2*, *VCAM1*, *FBN1*, *COL3A1*, *COL5A1*, *MMP2*, and *LOX*. TGF-β1 secreted from both cardiomyocytes and fibroblasts has been regarded as one of the key downstream effectors of the renin-angiotensin pathway that promotes atrial fibrosis. Both angiotensin and TGF-β are involved in a positive feedback mechanism by virtue of their autocrine and paracrine actions (Rosenkranz, 2004). The TGF-β1 signaling pathway is known to mainly act through the formation of a Smad 2/3/4 complex, which results in the upregulation of a wide spectrum of pro-fibrotic genes (Shi and Massagué, 2003; Thanigaimani et al., 2017). In addition to the Smad-dependent mechanism, several non-canonical pathways have been also implicated in TGF-β–induced cardiac remodeling. For example, the Akt/mTOR pathway is involved in TGF-β–induced collagen expression (Bujor et al., 2011; Wilkes and Leof, 2006), and JNK signaling crosstalks with TGF-β1 via the activation of key pro-fibrotic transcription factors such as c-Jun and NFκB (Mu et al., 2012; Thanigaimani et al., 2017). It is thus plausible that enhanced TGF-β1 expression and signaling as a key upstream regulator may account for the extensive alterations in the expression of fibrosis-related genes in RA induced by SNX.

Induction of *ACTA2* and *FN1*, coding for α-smooth muscle actin (α-SMA) and fibronectin 1, respectively is indicative of adverse cardiac remodeling as these factors are mainly expressed in myofibroblasts, and their expression indicates cardiac fibroblast proliferation and activation (Ge et al., 2018; Shinde et al., 2017; Weber et al., 2013). The normal myocardium contains a large number of fibroblast-like cells that remain quiescent in the absence of an injury. However, injuries causing cardiomyocyte loss can induce the conversion of cardiac fibroblasts into activated α-SMA–positive myofibroblasts, irrespective of the occurrence of cell loss at the macroscopic or microscopic level. Activated cardiac fibroblasts then secrete ECM proteins as well as autocrine/paracrine factors, such as fibronectin, fibrillary collagen, and CTGF, thereby protecting the cardiac chamber from adverse remodeling and the heart from a catastrophic rupture. Despite the reparative roles, excessive or prolonged cardiac fibroblast activation leads to fibrosis via excess fibrillar collagen deposition and then disrupts the architecture of the native myocardium (Pinto et al., 2016; Weber et al., 2013). Considering the fact that cardiac fibrosis is recognized as a primary contributor to heart failure, cardiac fibroblast proliferation or activation may underlie the increased risk of heart failure among patients with chronic SND.

As noted earlier, SND and AF frequently coexist and interact to initiate each other although the underlying mechanisms that link them are not fully defined (John and Kumar, 2016). Growing evidence suggests that AF can cause anatomical and/or electrophysiological remodeling within the SN

and surrounding atrial tissues leading to SND development. For example, animal AF models stimulated by persistent rapid atrial pacing resulted in SND characterized by prolonged SN recovery time and slow intrinsic HR along with atrial fibrosis (He et al., 2016; Morillo et al., 1995; Mulla et al., 2019; Wijffels et al., 1995). In contrast, we demonstrated that the SNX employed to recapitulate permanent SND caused by intrinsic factors led to atrial fibrosis within a week regardless of the AF onset. Indeed, both clinical and experimental findings support the hypothesis that prolonged impairment of SN function could be linked to the onset of atrial fibrosis independent of AF. In agreement with our results, atrial fibrosis is commonly observed among different SNX models generated using chemical reagents or genetic strategies (Herrmann et al., 2011; Zhong et al., 2018). More importantly, patients with conditions associated with atrial remodeling and atrial stretch exhibit impaired SN functions even in the absence of atrial arrhythmias (Medi et al., 2012; Morton et al., 2003; Sanders et al., 2004). However, it is unclear whether SNX-induced bradycardia causes fibrotic alterations in atrial tissues, while bradycardia itself has been proposed to facilitate the development of conditions conducive to AF occurrence (Amasyali et al., 2014). Nevertheless, initiation of fibrotic remodeling in atrial tissues by SNX may provide an additional link between SND and AF because fibrosis-induced disorganization of electric coupling in the atrium results in increased automaticity and atrial ectopy, thereby potentiating cardiac arrhythmias (Platonov, 2017; Xie et al., 2009).

Of interest, a robust induction of *POSTN* mRNA expression throughout myocardial tissues should be highlighted. Periostin is a secreted 90 kDa protein that constitutes the non-structural component of ECM, and is considered as an important matricellular factor regulating cardiac development (Landry et al., 2018). More importantly, it plays a key role in the crosstalk between the cells and surrounding ECM, and is associated with fibroproliferative diseases of the myocardium. Indeed, growing evidence suggests the mediatory roles of periostin in the etiology of various cardiovascular diseases (Lindner et al., 2005; Markwald et al., 2010; Wu et al., 2016; Zhao et al., 2014). Induction of periostin expression in the cardiovascular system has primarily been attributed to the signaling pathway induced by members of the TGF-β superfamily (Landry et al., 2018). Various extracellular stimuli including cytokines/chemokines, mechanical stress, and alterations in the matrix composition can induce periostin expression directly or indirectly through TGF-β signaling. For example, treatment of cultured primary cardiac fibroblasts with recombinant TGF-β1 induces periostin expression in a Smad-dependent manner (Snider et al., 2008), whereas acute myocardial infarction (MI)-associated periostin expression is significantly attenuated by neutralizing anti-TGF-β antibodies (Iekushi et al., 2007). Despite the well-established link between periostin expression and TGF-β signaling, a clear explanation of SND-induced periostin expression is not simple because the correlation between periostin and TGF-β expression is found only in the atrial tissues, but not in the ventricular regions as shown in Fig. 4. It is plausible that TGF-β produced in the atrial regions may be responsible for the induction of periostin expression throughout myocardial tissues. Impaired natriuretic peptide signaling raises an alternative possibility leading to increased periostin expression in ventricular tissues in the present study. It has been proposed that atrial natriuretic peptide (ANP) negatively regulates periostin expression in several cell types (Li et al., 2007; Wang et al., 2003). For example, steady-state periostin expression in the LV is higher in ANP-deficient mice than that in wild-type controls, and transverse aortic constriction induces more robust upregulation of *POSTN* mRNA expression in the LV tissues of the mutant mice (Wang et al., 2003), while NPR1 null mice show marginal changes in cardiac TGF-β expression (Ellmers et al., 2007). It has also been shown that knocking-down NPR1 expression resulted in an increase in the levels of basal phosphorylated Smad2 and an exaggerated response to TGF-β1 stimulation in both atrial and ventricular myofibroblast cultures (Rahmutula et al., 2019). It is therefore, plausible that impaired ANP signaling would be responsible for induction of periostin expression throughout atrial and ventricular regions in our SNX animals in contrast to atrial-specific increases in TGF-β1 protein levels.

Secreted periostin can physically or functionally interact with various ECM proteins such as tenascin C (TNC), a subset of collagens, and lysyl oxidase (coded by *LOX*), thereby stimulating integrin signaling and further establishing pro-fibrotic changes in a feed-forward manner (Kii et al., 2010; Li et al., 2010; Maruhashi et al., 2010; Norris et al., 2007). Indeed, mRNA levels for well-established transcriptional targets of integrin signaling, including *LOX*, *TNC*, *CTGF*, and several *COL* genes were significantly augmented in the SNX RA tissues (Figs. 2 and 3). These results again support the hypothesis that periostin can be a pivotal mediator of the fibrotic phenotypes caused by the SND. In this respect, several studies have suggested the therapeutic implications of periostin in cardiovascular diseases associated with cardiac fibrosis. It was initially demonstrated that genetic abrogation of *POSTN* in mice led to an increased risk of ventricular rupture after an MI, but surviving mice showed less fibrosis and good ventricular performance (Oka et al., 2007; Shimazaki et al., 2008). Mice lacking periostin also show less fibrosis and hypertrophy in response to long-term pressure overload (Oka et al., 2007). Conversely, heart-specific periostin overexpression in mice protects them from ventricular rupture by MI, but induces spontaneous cardiac hypertrophy with aging (Oka et al., 2007; Shimazaki et al., 2008). Integrin and focal adhesion kinase (FAK) signaling-induced cell migration has been shown to underlie the post-MI cardiac healing by periostin (Shimazaki et al., 2008). Furthermore, a neutralizing antibody, which selectively inhibits the full-length periostin, but not significantly the shorter isoforms, decreases the infarcted and fibrotic areas of the myocardium without increasing post-MI cardiac ruptures. This finding implies that the inhibition of periostin action has therapeutic potential with respect to treating cardiac fibrosis-associated diseases, including post-MI cardiac remodeling (Taniyama et al., 2016).

In conclusion, the present study demonstrates that impaired SN function can directly lead to adverse structural remodeling of the RA tissue through activation of pro-fibrotic signaling and provides valuable information about the molecular signatures underlying this process. Although

the renin-angiotensin II pathway-dependent TGF-β signaling activation has been implicated in atrial fibrosis initiation, our findings strongly suggest that periostin may have an additional role in not only mediating, but also reinforcing the feedback mechanism underlying TGF-β signaling-mediated aberrant ECM deposition. Notably, periostin profiles of body fluids have been proposed as potential biomarkers for several human diseases particularly those linked with inflammatory or fibrotic responses, such as asthma, skin-related disorders, and renal diseases (Inoue et al., 2016; Prakoura and Chatziantoniou, 2017; Yamaguchi, 2014). The remarkable up-regulation of periostin expression in association with cardiac fibrosis raises the possibility of its diagnostic application as a less invasive biomarker for cardiac dysfunctions in addition to its therapeutic potential.

Note: Supplementary information is available on the Molecules and Cells website (www.molcells.org).

ACKNOWLEDGMENTS

This work was supported by the Ministry of Science and ICT through the National Research Foundation of Korea (NRF-2015M3A9E7029176 and NRF-2016M3C7A1904340 to G.H.S., and NRF-2017R1C1B5017935 to S.Y.R.). J.S. and G.H.S. were supported by the Korea University Research Grant.

AUTHOR CONTRIBUTIONS

S.Y.R. and G.H.S. conceived the study. S.Y.R., J.Y.K., H.K.C., H.Y.L., Y.P., K.N.L., J.S., and J.I.C. performed the experiments. S.Y.R., J.Y.K., Y.H.K., and G.H.S. analyzed the results and wrote the paper.

CONFLICT OF INTEREST

The authors have no potential conflicts of interest to disclose.

ORCID

Seung-Young Roh https://orcid.org/0000-0002-0854-9079
Ji Yeon Kim https://orcid.org/0000-0002-0486-9948
Hyo Kyeong Cha https://orcid.org/0000-0002-0820-7714
Hye Young Lim https://orcid.org/0000-0003-1266-2645
Youngran Park https://orcid.org/0000-0002-8621-1399
Kwang-No Lee https://orcid.org/0000-0002-7430-415X
Jaemin Shim https://orcid.org/0000-0001-8251-1522
Jong-Il Choi https://orcid.org/0000-0001-6617-508X
Young-Hoon Kim https://orcid.org/0000-0002-4254-647X
Gi Hoon Son https://orcid.org/0000-0001-9758-5903

REFERENCES

Abe, K., Machida, T., Sumitomo, N., Yamamoto, H., Ohkubo, K., Watanabe, I., Makiyama, T., Fukae, S., Kohno, M., Harrell, D.T., et al. (2014). Sodium channelopathy underlying familial sick sinus syndrome with early onset and predominantly male characteristics. Circ. Arrhythm. Electrophysiol. *7*, 511-517.

Alonso, A., Jensen, P.N., Lopez, F.L., Chen, L.Y., Psaty, B.M., Folsom, A.R., and Heckbert, S.R. (2014). Association of sick sinus syndrome with incident cardiovascular disease and mortality: the atherosclerosis risk in communities study and cardiovascular health study. PLoS One *9*, e109662.

Amasyali, B., Kilic, A., and Kilit, C. (2014). Sinus node dysfunction and atrial fibrillation: which one dominates? Int. J. Cardiol. *175*, 379-380.

Andersen, H.R., Nielsen, J.C., Thomsen, P.E., Thuesen, L., Mortensen, P.T., Vesterlund, T., and Pedersen, A.K. (1997). Long-term follow-up of patients from a randomised trial of atrial versus ventricular pacing for sick-sinus syndrome. Lancet *350*, 1210-1216.

Assayag, P., Carre, F., Chevalier, B., Delcayre, C., Mansier, P., and Swynghedauw, B. (1997). Compensated cardiac hypertrophy: arrhythmogenicity and the new myocardial phenotype. I. fibrosis. Cardiovasc. Res. *34*, 439-444.

Bernstein, A.D. and Parsonnet, V. (1996). Survey of cardiac pacing and defibrillation in the United States in 1993. Am. J. Cardiol. *78*, 187-196.

Bujor, A.M., Asano, Y., Haines, P., Lafyatis, R., and Trojanowska, M. (2011). The c-Abl tyrosine kinase controls protein kinase Cdelta-induced Fli-1 phosphorylation in human dermal fibroblasts. Arthritis Rheum. *63*, 1729-1737.

Chung, S., Kim, I.H., Lee, D., Park, K., Kim, J.Y., Lee, Y.K., Kim, E.J., Lee, H.W., Choi, J.S., Son, G.H., et al. (2016). The role of inositol 1,4,5-trisphosphate 3-kinase A in regulating emotional behavior and amygdala function. Sci. Rep. *6*, 23757.

Chung, S., Lee, E.J., Cha, H.K., Kim, J., Kim, D., Son, G.H., and Kim, K. (2017). Cooperative roles of the suprachiasmatic nucleus central clock and the adrenal clock in controlling circadian glucocorticoid rhythm. Sci. Rep. *7*, 46404.

Connolly, S.J., Kerr, C.R., Gent, M., Roberts, R.S., Yusuf, S., Gillis, A.M., Sami, M.H., Talajic, M., Tang, A.S., Klein, G.J., et al. (2000). Effects of physiologic pacing versus ventricular pacing on the risk of stroke and death due to cardiovascular causes. Canadian trial of physiologic pacing investigators. N. Engl. J. Med. *342*, 1385-1391.

Dobrzynski, H., Boyett, M.R., and Anderson, R.H. (2007). New insights into pacemaker activity: promoting understanding of sick sinus syndrome. Circulation *115*, 1921-1932.

Ellmers, L.J., Scott, N.J., Piuhola, J., Maeda, N., Smithies, O., Frampton, C.M., Richards, A.M., and Cameron, V.A. (2007). Npr1-regulated gene pathways contributing to cardiac hypertrophy and fibrosis. J. Mol. Endocrinol. *38*, 245.

Ge, J., Burnier, L., Adamopoulou, M., Kwa, M.Q., Schaks, M., Rottner, K., and Brakebusch, C. (2018). RhoA, Rac1, and Cdc42 differentially regulate alphaSMA and collagen I expression in mesenchymal stem cells. J. Biol. Chem. *293*, 9358-9369.

He, X., Zhang, K., Gao, X., Li, L., Tan, H., Chen, J., and Zhou, Y. (2016). Rapid atrial pacing induces myocardial fibrosis by down-regulating Smad7 via microRNA-21 in rabbit. Heart Vessels *31*, 1696-1708.

Herrmann, S., Fabritz, L., Layh, B., Kirchhof, P., and Ludwig, A. (2011). Insights into sick sinus syndrome from an inducible mouse model. Cardiovasc. Res. *90*, 38-48.

Iekushi, K., Taniyama, Y., Azuma, J., Katsuragi, N., Dosaka, N., Sanada, F., Koibuchi, N., Nagao, K., Ogihara, T., and Morishita, R. (2007). Novel mechanisms of valsartan on the treatment of acute myocardial infarction through inhibition of the antiadhesion molecule periostin. Hypertension *49*, 1409-1414.

Inoue, T., Akashi, K., Watanabe, M., Ikeda, Y., Ashizuka, S., Motoki, T., Suzuki, R., Sagara, N., Yanagida, N., Sato, S., et al. (2016). Periostin as a biomarker for the diagnosis of pediatric asthma. Pediatr. Allergy Immunol. *27*, 521-526.

Jensen, P.N., Gronroos, N.N., Chen, L.Y., Folsom, A.R., deFilippi, C., Heckbert, S.R., and Alonso, A. (2014). Incidence of and risk factors for sick sinus syndrome in the general population. J. Am. Coll. Cardiol. *64*, 531-538.

John, R.M. and Kumar, S. (2016). Sinus node and atrial arrhythmias. Circulation *133*, 1892-1900.

Joung, B., Lin, S.F., Chen, Z., Antoun, P.S., Maruyama, M., Han, S., Piccirillo, G., Stucky, M., Zipes, D.P., Chen, P.S., et al. (2010). Mechanisms of sinoatrial

node dysfunction in a canine model of pacing-induced atrial fibrillation. Heart Rhythm *7*, 88-95.

Kii, I., Nishiyama, T., Li, M., Matsumoto, K., Saito, M., Amizuka, N., and Kudo, A. (2010). Incorporation of tenascin-C into the extracellular matrix by periostin underlies an extracellular meshwork architecture. J. Biol. Chem. *285*, 2028-2039.

Kim, J.Y., Lim, H.Y., Shin, S.E., Cha, H.K., Seo, J.H., Kim, S.K., Park, S.H., and Son, G.H. (2018). Comprehensive transcriptome analysis of Sarcophaga peregrina, a forensically important fly species. Sci. Data *5*, 180220.

Lamas, G.A., Lee, K.L., Sweeney, M.O., Silverman, R., Leon, A., Yee, R., Marinchak, R.A., Flaker, G., Schron, E., Orav, E.J., et al. (2002). Ventricular pacing or dual-chamber pacing for sinus-node dysfunction. N. Engl. J. Med. *346*, 1854-1862.

Landry, N.M., Cohen, S., and Dixon, I.M.C. (2018). Periostin in cardiovascular disease and development: a tale of two distinct roles. Basic Res. Cardiol. *113*, 1.

Li, G., Jin, R., Norris, R.A., Zhang, L., Yu, S., Wu, F., Markwald, R.R., Nanda, A., Conway, S.J., Smyth, S.S., et al. (2010). Periostin mediates vascular smooth muscle cell migration through the integrins alphavbeta3 and alphavbeta5 and focal adhesion kinase (FAK) pathway. Atherosclerosis *208*, 358-365.

Li, G., Liu, E., Liu, T., Wang, J., Dai, J., Xu, G., Korantzopoulos, P., and Yang, W. (2011). Atrial electrical remodeling in a canine model of sinus node dysfunction. Int. J. Cardiol. *146*, 32-36.

Li, P., Oparil, S., Novak, L., Cao, X., Shi, W., Lucas, J., and Chen, Y.F. (2007). ANP signaling inhibits TGF-beta-induced Smad2 and Smad3 nuclear translocation and extracellular matrix expression in rat pulmonary arterial smooth muscle cells. J. Appl. Physiol. *102*, 390-398.

Lindner, V., Wang, Q., Conley, B.A., Friesel, R.E., and Vary, C.P. (2005). Vascular injury induces expression of periostin: implications for vascular cell differentiation and migration. Arterioscler. Thromb. Vasc. Biol. *25*, 77-83.

Liu, R.X., Wang, Y.L., Li, H.B., Wang, N.N., Bao, M.J., and Xu, L.Y. (2012). Comparative study between original and traditional method in establishing a chronic sinus node damage model in rabbit. J. Appl. Physiol. *113*, 1802-1808.

Markwald, R.R., Norris, R.A., Moreno-Rodriguez, R., and Levine, R.A. (2010). Developmental basis of adult cardiovascular diseases: valvular heart diseases. Ann. N. Y. Acad. Sci. *1188*, 177-183.

Maruhashi, T., Kii, I., Saito, M., and Kudo, A. (2010). Interaction between periostin and BMP-1 promotes proteolytic activation of lysyl oxidase. J. Biol. Chem. *285*, 13294-13303.

Medi, C., Kalman, J.M., Ling, L.H., Teh, A.W., Lee, G., Lee, G., Spence, S.J., Kaye, D.M., and Kistler, P.M. (2012). Atrial electrical and structural remodeling associated with longstanding pulmonary hypertension and right ventricular hypertrophy in humans. J. Cardiovasc. Electrophysiol. *23*, 614-620.

Morillo, C.A., Klein, G.J., Jones, D.L., and Guiraudon, C.M. (1995). Chronic rapid atrial pacing. Structural, functional, and electrophysiological characteristics of a new model of sustained atrial fibrillation. Circulation *91*, 1588-1595.

Morton, J.B., Sanders, P., Vohra, J.K., Sparks, P.B., Morgan, J.G., Spence, S.J., Grigg, L.E., and Kalman, J.M. (2003). Effect of chronic right atrial stretch on atrial electrical remodeling in patients with an atrial septal defect. Circulation *107*, 1775-1782.

Mu, Y., Gudey, S.K., and Landstrom, M. (2012). Non-Smad signaling pathways. Cell Tissue Res. *347*, 11-20.

Mulla, W., Hajaj, B., Elyagon, S., Mor, M., Gillis, R., Murninkas, M., Klapper-Goldstein, H., Plaschkes, I., Chalifa-Caspi, V., Etzion, S., et al. (2019). Rapid atrial pacing promotes atrial fibrillation substrate in unanesthetized instrumented rats. Front. Physiol. *10*, 1218.

Nielsen, J.C., Thomsen, P.E., Hojberg, S., Moller, M., Vesterlund, T., Dalsgaard, D., Mortensen, L.S., Nielsen, T., Asklund, M., Friis, E.V., et al. (2011). A comparison of single-lead atrial pacing with dual-chamber pacing in sick sinus syndrome. Eur. Heart J. *32*, 686-696.

Norris, R.A., Damon, B., Mironov, V., Kasyanov, V., Ramamurthi, A., Moreno-Rodriguez, R., Trusk, T., Potts, J.D., Goodwin, R.L., Davis, J., et al. (2007). Periostin regulates collagen fibrillogenesis and the biomechanical properties of connective tissues. J. Cell. Biochem. *101*, 695-711.

Oka, T., Xu, J., Kaiser, R.A., Melendez, J., Hambleton, M., Sargent, M.A., Lorts, A., Brunskill, E.W., Dorn, G.W., 2nd, Conway, S.J., et al. (2007). Genetic manipulation of periostin expression reveals a role in cardiac hypertrophy and ventricular remodeling. Circ. Res. *101*, 313-321.

Pinto, A.R., Ilinykh, A., Ivey, M.J., Kuwabara, J.T., D'Antoni, M.L., Debuque, R., Chandran, A., Wang, L., Arora, K., Rosenthal, N.A., et al. (2016). Revisiting cardiac cellular composition. Circ. Res. *118*, 400-409.

Platonov, P.G. (2017). Atrial fibrosis: an obligatory component of arrhythmia mechanisms in atrial fibrillation? J. Geriatr. Cardiol. *14*, 233-237.

Prakoura, N. and Chatziantoniou, C. (2017). Periostin and discoidin domain receptor 1: new biomarkers or targets for therapy of renal disease. Front. Med. (Lausanne) *4*, 52.

Rahmutula, D., Zhang, H., Wilson, E.E., and Olgin, J.E. (2019). Absence of natriuretic peptide clearance receptor attenuates TGF-β1-induced selective atrial fibrosis and atrial fibrillation. Cardiovasc. Res. *115*, 357.

Rosenkranz, S. (2004). TGF-beta1 and angiotensin networking in cardiac remodeling. Cardiovasc. Res. *63*, 423-432.

Sanders, P., Morton, J.B., Kistler, P.M., Spence, S.J., Davidson, N.C., Hussin, A., Vohra, J.K., Sparks, P.B., and Kalman, J.M. (2004). Electrophysiological and electroanatomic characterization of the atria in sinus node disease: evidence of diffuse atrial remodeling. Circulation *109*, 1514-1522.

Shi, Y. and Massagué, J. (2003). Mechanisms of TGF-beta signaling from cell membrane to the nucleus. Cell *113*, 685-700.

Shimazaki, M., Nakamura, K., Kii, I., Kashima, T., Amizuka, N., Li, M., Saito, M., Fukuda, K., Nishiyama, T., Kitajima, S., et al. (2008). Periostin is essential for cardiac healing after acute myocardial infarction. J. Exp. Med. *205*, 295-303.

Shinde, A.V., Humeres, C., and Frangogiannis, N.G. (2017). The role of alpha-smooth muscle actin in fibroblast-mediated matrix contraction and remodeling. Biochim. Biophys. Acta Mol. Basis Dis. *1863*, 298-309.

Silver, M.A., Pick, R., Brilla, C.G., Jalil, J.E., Janicki, J.S., and Weber, K.T. (1990). Reactive and reparative fibrillar collagen remodelling in the hypertrophied rat left ventricle: two experimental models of myocardial fibrosis. Cardiovasc. Res. *24*, 741-747.

Snider, P., Hinton, R.B., Moreno-Rodriguez, R.A., Wang, J., Rogers, R., Lindsley, A., Li, F., Ingram, D.A., Menick, D., Field, L., et al. (2008). Periostin is required for maturation and extracellular matrix stabilization of noncardiomyocyte lineages of the heart. Circ. Res. *102*, 752-760.

Taniyama, Y., Katsuragi, N., Sanada, F., Azuma, J., Iekushi, K., Koibuchi, N., Okayama, K., Ikeda-Iwabu, Y., Muratsu, J., Otsu, R., et al. (2016). Selective blockade of periostin exon 17 preserves caediac performance in acute myocardial infarction. Hypertension *67*, 356-361.

Thanigaimani, S., Lau, D.H., Agbaedeng, T., Elliott, A.D., Mahajan, R., and Sanders, P. (2017). Molecular mechanisms of atrial fibrosis: implications for the clinic. Expert Rev. Cardiovasc. Ther. *15*, 247-256.

Wang, D., Oparil, S., Feng, J.A., Li, P., Perry, G., Chen, L.B., Dai, M., John, S.W., and Chen, Y.F. (2003). Effects of pressure overload on extracellular matrix expression in the heart of the atrial natriuretic peptide-null mouse. Hypertension *42*, 88-95.

Weber, K.T., Sun, Y., Bhattacharya, S.K., Ahokas, R.A., and Gerling, I.C. (2013). Myofibroblast-mediated mechanisms of pathological remodelling of the heart. Nat. Rev. Cardiol. *10*, 15-26.

Wijffels, M.C., Kirchhof, C.J., Dorland, R., and Allessie, M.A. (1995).

Atrial fibrillation begets atrial fibrillation. A study in awake chronically instrumented goats. Circulation *92*, 1954-1968.

Wilkes, M.C. and Leof, E.B. (2006). Transforming growth factor beta activation of c-Abl is independent of receptor internalization and regulated by phosphatidylinositol 3-kinase and PAK2 in mesenchymal cultures. J. Biol. Chem. *281*, 27846-27854.

Wu, H., Chen, L., Xie, J., Li, R., Li, G.N., Chen, Q.H., Zhang, X.L., Kang, L.N., and Xu, B. (2016). Periostin expression induced by oxidative stress contributes to myocardial fibrosis in a rat model of high salt-induced hypertension. Mol. Med. Rep. *14*, 776-782.

Xie, Y., Garfinkel, A., Camelliti, P., Kohl, P., Weiss, J.N., and Qu, Z. (2009). Effects of fibroblast-myocyte coupling on cardiac conduction and vulnerability to reentry: a computational study. Heart Rhythm *6,* 1641-1649.

Yamaguchi, Y. (2014). Periostin in skin tissue skin-related diseases. Allergol. Int. *63*, 161-170.

Zhao, S., Wu, H., Xia, W., Chen, X., Zhu, S., Zhang, S., Shao, Y., Ma, W., Yang, D., and Zhang, J. (2014). Periostin expression is upregulated and associated with myocardial fibrosis in human failing hearts. J. Cardiol. *63*, 373-378.

Zhao, Y., Wang, C., Wang, C., Hong, X., Miao, J., Liao, Y., Zhou, L., and Liu, Y. (2018). An essential role for Wnt/beta-catenin signaling in mediating hypertensive heart disease. Sci. Rep. *8*, 8996.

Zhong, H., Wang, T., Lian, G., Xu, C., Wang, H., and Xie, L. (2018). TRPM7 regulates angiotensin II-induced sinoatrial node fibrosis in sick sinus syndrome rats by mediating Smad signaling. Heart Vessels *33*, 1094-1105.

Ziyadeh-Isleem, A., Clatot, J., Duchatelet, S., Gandjbakhch, E., Denjoy, I., Hidden-Lucet, F., Hatem, S., Deschenes, I., Coulombe, A., Neyroud, N., et al. (2014). A truncating SCN5A mutation combined with genetic variability causes sick sinus syndrome and early atrial fibrillation. Heart Rhythm *11*, 1015-1023.